Available online at www.sciencedirect.com

SciVerse ScienceDirect

Scripta Materialia 69 (2013) 553–556

Scripta MATERIALIA

www.elsevier.com/locate/scriptamat

A new CoFe-based bulk metallic glasses with high thermoplastic forming ability

Qikui Man,[a,*] Akihisa Inoue,[a,b] Yaqiang Dong,[a] Jian Qiang,[a] Chengliang Zhao[a] and Baolong Shen[c,*]

[a]*Key Laboratory of Magnetic Materials and Devices, Ningbo Institute of Materials Technology & Engineering, Chinese Academy of Sciences, 519 Zhuanshi Road, Zhenhai District, Ningbo, Zhejiang 315201, China*
[b]*International Institute of Green Materials, Josai International University, Togane, 283-8555, Japan*
[c]*School of Materials Science and Engineering, Southeast University, Nanjing 211189, China*

Received 8 April 2013; revised 29 June 2013; accepted 2 July 2013
Available online 11 July 2013

The $(Co_{0.5}Fe_{0.5})_{62}Nb_6M_2B_{30}$ (M = Er, Tb, Y or Dy) bulk metallic glasses with a large supercooled liquid region up to 130 K are reported. Their high processing ability was demonstrated by simple microreplication experiments. In addition, this bulk metallic glass system exhibits a high fracture strength of up to 4750 MPa and a Vickers hardness of up to 1258, together with good soft-magnetic properties. Combining good mechanical properties with high thermoplastic forming ability, these bulk metallic glasses have potential for use in engineering applications.

Keywords: Metallic glass; Thermoplastic forming ability; Mechanical properties; Magnetic properties

The development of micromachines, microelectronics, biomedical devices and microelectromechanical systems has been required to fabricate microparts (<1 mm) with superior mechanical properties and high dimensional accuracy in complex geometries. While metals are widely used as structural materials, most of them cannot be processed into the shape required to perform specialized functions because of the intrinsic disadvantage caused by crystalline defects and grain boundaries [1]. Compared with metals, plastics and glasses exhibit versatile processability, but their low strength has hampered their use as structural parts. Bulk metallic glasses (BMGs), in contrast, display superhigh strength, excellent corrosion resistances and soft-magnetic properties (for Fe- and Co-based BMGs) [2–4]. In addition, BMGs with high thermal stability can also be formed thermoplastically, like plastics. Thermoplastic forming (TPF) takes place in a supercooled liquid region (SCLR), where the viscosity of the BMG drops significantly, allowing it to flow under a small applied pressure. Like plastics, some BMGs can even access an ideal processing window of forming pressure, which lies between 10^{-5} and 1 MPa [5]. Consequently, BMGs can be considered high-strength metals that can be processed like plastics in an SCLR [5]. Therefore, low viscosity in the SCLR, an amorphous structure down to the atomic scale, excellent mechanical properties and relatively small shrinkage make some BMGs ideal candidates for TPF in small-scale applications.

Considering the metastable nature of BMGs, the main challenge associated with TPF in an SCLR is to avoid crystallization. Therefore, most studies of TPF focus on BMGs with high thermal stability, such as those based on Pt [6], Pd [7], Zr [1,8], Au [9] or Ce [10], which are typically quantified by the range of the SCLR (ΔT_x), bounded between the glass transition temperature (T_g) and the crystallization temperature (T_x). Recently, precise microstructures of Pt-based BMG on length scales ranging down to ten nanometers have been successfully processed [6]. These glassy alloys mentioned previously exhibit relatively low T_g and fracture strength (σ_f), which make the TPF process more easy. Fe- and Co-based BMGs exhibit high T_g and σ_f; for example, the T_g and σ_f of $Co_{43}Fe_{20}Ta_{5.5}B_{31.5}$ BMG are 910 K and 5185 MPa, respectively [11]. Thus the BMG could be used in high-temperature conditions and the high σ_f

* Corresponding authors. Tel.: +86 574 86685027; fax: +86 574 87911392; e-mail addresses: manqk@nimte.ac.cn (Q. Man); blshen@seu.edu.cn (B. Shen)

1359-6462/$ - see front matter © 2013 Acta Materialia Inc. Published by Elsevier Ltd. All rights reserved.
http://dx.doi.org/10.1016/j.scriptamat.2013.07.002

may confer good wear and abrasion resistance [12]. However, there are few reports on the TPF of Fe- and Co-based BMGs, because very few of them simultaneously exhibit the large SCLR and high glass-forming ability (GFA) that are required for the TPF process.

With the aim of synthesizing a new CoFe-based BMG with a large SCLR and a high GFA, we focused on $Co_{43}Fe_{20}Ta_{5.5}B_{31.5}$ BMG, owing to its larger SCLR of 72 K as well as high σ_f and hardness [12]. To further increase the GFA of the alloy, Ta was substituted by Nb, because Nb is effective in enhancing the GFA of CoFe-based BMG [13]. The effects of the Co to Fe concentration ratio and the Nb content on the range of SCLR were then investigated, and it was found that the glassy alloy with the composition of $(Co_{0.5}Fe_{0.5})_{64}Nb_6B_{30}$ shows a ΔT_x of 80 K. In order to further enlarge the SCLR, 2 at.% rare-earth element (Er, Tb, Y or Dy) was added to the CoFeNbB quaternary glassy alloy, because these elements have large atomic radii [14] and negative mixing enthalpies among Co, Fe, Nb and B [15]. As a result, the $(Co_{0.5}Fe_{0.5})_{62}Nb_6M_2B_{30}$ (M = Er, Tb, Y or Dy) BMGs with a large SCLR up to 130 K were synthesized.

Alloy ingots were made by alloying high-purity elements in an arc furnace under an argon atmosphere. Cylindrical alloy rods with diameters up to 4 mm were produced by the copper mold casting method. The glassy structure of the as-cast and processed samples was examined by X-ray diffraction (XRD) using Cu K_α radiation. The thermal stability associated with T_g, T_x and ΔT_x was examined by differential scanning calorimetry (DSC) using a Netzsch 404C calorimeter. The mechanical properties of σ_f were measured by compression testing with a UTM 5105 testing machine. Cylindrical test samples, 2 mm in diameter and 4 mm in height, were used and the strain rate was $5 \times 10^{-4}\ s^{-1}$. The Vickers hardness (H_v) was measured with a hardness tester under a load of 9.8 N. The magnetic properties of saturation magnetization (I_s), coercive force (H_c) and effective permeability (μ_e) were measured with a vibrating sample magnetometer (VSM) under an applied field of 800 kA m^{-1}, a B-H loop tracer under a field of 800 A m^{-1} and an impedance analyzer under a field of 1 A m^{-1}, respectively.

As shown in Figure 1, T_g is 890 K for the $(Co_{0.5}Fe_{0.5})_{64}Nb_6B_{30}$ glassy alloy and increases to 900 K with the addition of Er, Tb, Y or Dy. ΔT_x is 80 K for the $(Co_{0.5}Fe_{0.5})_{64}Nb_6B_{30}$ glassy alloy and increases to 118, 120, 123 and 130 K with the addition of Er, Tb, Y or Dy, respectively. The liquidus temperature (T_l) of the $(Co_{0.5}Fe_{0.5})_{64}Nb_6B_{30}$ glassy alloy decreases from 1490 K to 1438, 1436, 1440 and 1437 K, respectively. The reduced glass transition temperature ($T_{rg} = T_g/T_l$) increases from 0.597 to 0.626, 0.629, 0.627 and 0.625 with the addition of 2 at.% Er, Tb, Y or Dy, respectively. Similarly, the parameter γ ($\gamma = T_x/(T_g + T_l)$) [16] increases from 0.407 to 0.434, 0.437, 0.438 and 0.440, respectively.

The cylindrical alloy rods were successfully produced over the whole range of compositions and the amorphous structure of the as-cast samples was examined by XRD. It was found that the $(Co,Fe,Nb)_{23}B_6$ and $(Co,Fe)_2B$ phases precipitate from the glassy phase in a 1 mm diameter rod of $(Co_{0.5}Fe_{0.5})_{64}Nb_6B_{30}$ alloy. Only a broad peak without any crystalline peaks can be seen in the XRD patterns for the alloys containing Y, Dy, Tb or Er, indicating that the critical diameter for formation of a single glassy phase is 3 mm for these glassy alloys. In this study, it was clarified that the dissolution of 2 at.% Er, Tb, Y or Dy can effectively extend the SCLR and enhance the GFA for the $(Co_{0.5}Fe_{0.5})_{62}Nb_6M_2B_{30}$ BMG system.

These BMGs of M = Er, Tb, Y or Dy exhibit superhigh σ_f values of 4350, 4430, 4620 and 4750 MPa, respectively, and high H_v values of 1236, 1243, 1256 and 1258, respectively, at room temperature (RT). It has been reported that the σ_f at RT is in the range of 1500–2000 MPa for Zr-based BMGs [13], about 1500 MPa for Pd- and Pt-based BMGs [13], and about 500 MPa for Ce-based BMGs [10]. Compared to such BMGs, the $(Co_{0.5}Fe_{0.5})_{62}Nb_6M_2B_{30}$ BMGs may exhibit excellent durability and wear resistance due to their good mechanical properties for engineering applications [12].

The temperature dependence on the strength of $(Co_{0.5}Fe_{0.5})_{62}Nb_6Dy_2B_{30}$ BMG was also investigated. Figure 2 shows compressive stress–strain curves for the 2 mm as-cast rods at different temperatures. This

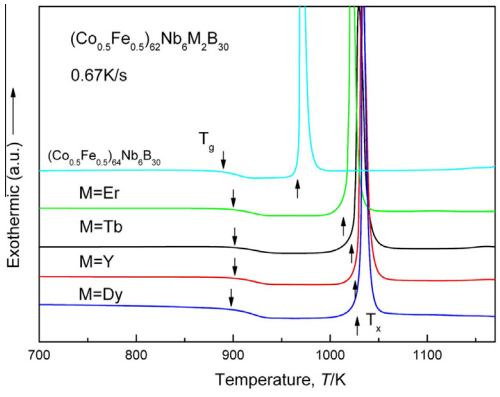

Figure 1. DSC curves of $(Co_{0.5}Fe_{0.5})_{62}Nb_6M_2B_{30}$ (M = Er, Tb, Y or Dy) BMGs and $(Co_{0.5}Fe_{0.5})_{62}Nb_8B_{30}$ glassy alloy.

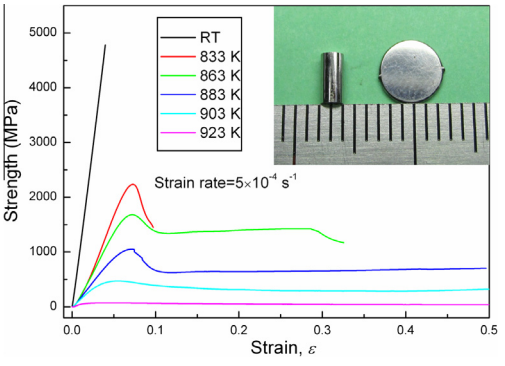

Figure 2. The compressive stress–strain curves of 2 mm $(Co_{0.5}Fe_{0.5})_{62}Nb_6Dy_2B_{30}$ as-cast rods at deferent temperature. The inset figure shows photographs of the starting sample and the final sample compressed at 923 K.

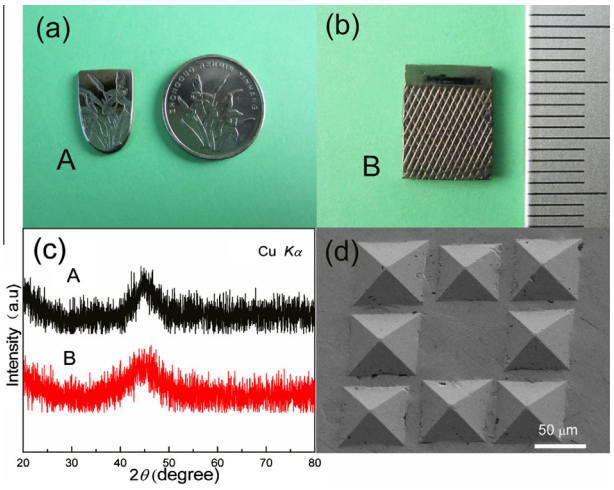

Figure 3. (a) The pattern of a Chinese dime coin imprinted into the $(Co_{0.5}Fe_{0.5})_{62}Nb_6Dy_2B_{30}$ BMG sheet at 953 K. (b) The reticular pattern impressed into this BMG sheet. (c) XRD patterns of the final samples A and B after the TPF process. (d) A diamond-shape pattern on a length scale of about 50 μm replicated on the BMG sheet.

BMG exhibits an σ_f of 4750 MPa at RT and about 2% elastic strain followed by fracture. It is brittle at RT; however, the compressive behavior completely changes to perfect superplasticity when the temperature rises to 923 K. When the temperature rises to near the T_g, the value of σ_f dramatically decreases, being just 0.8 MPa at 953 K at a strain rate 5×10^{-4} s^{-1}. The inset in Figure 2 shows photographs of the starting sample, with a diameter of 2 mm and height of 4 mm, and the final sample, which was compressed up to a height of 0.6 mm without cracking at 923 K, demonstrating good deformability of this BMG in an SCLR.

The highly viscous liquid of a BMG is metastable, hence the time of onset of crystallization is crucial for TPF in an SCLR. For the $(Co_{0.5}Fe_{0.5})_{62}Nb_6Dy_2B_{30}$ BMG, the time of onset of crystallization at 953 K was detected to be about 7 min using isothermal DSC. The high thermal stability of this BMG offers a wide enough processing time window for the TPF process. In order to perform the TPF experiments, $(Co_{0.5}Fe_{0.5})_{62}Nb_6Dy_2B_{30}$ BMG sheets with a thickness of 1 mm were prepared. Figure 3(a) presents the pattern of a Chinese dime coin imprinted into the $(Co_{0.5}Fe_{0.5})_{62}Nb_6Dy_2B_{30}$ BMG sheet at 953 K under a pressure of 30 MPa for 60 s. To prevent oxidation, all the samples and molds were wrapped up together with copper foil. It can be seen that sample A, of the coin pattern, was replicated successfully; even the scratches on the original dime are clearly reproduced. Sample B, of a reticular pattern impressed into the BMG sheet, is shown in Figure 3(b). The structures of the final samples A and B, after the TPF process, were examined by XRD, as shown in Figure 3(c). Only a broad peak without any crystalline peaks can be seen, indicating the fully glassy phase after the TPF process. Figure 3(d) represents diamond-shaped patterns, on length scales ranging down to micrometers, that are successfully replicated on the BMG sheet. These results indicate the good TPF ability of the $(Co_{0.5}Fe_{0.5})_{62}Nb_6Dy_2B_{30}$ BMG in an SCLR.

In addition, Fe- and Co-based ferromagnetic BMGs are promising candidates for ferromagnetic core materials owing to their high efficiency for energy transformation. We also measured the soft-magnetic properties of this glassy alloy system. Figure 4 shows the *I–H* hysteresis curves of $(Co_{0.5}Fe_{0.5})_{62}Nb_6M_2B_{30}$ (M = Er, Tb, Y or Dy) and $(Co_{0.5}Fe_{0.5})_{62}Nb_8B_{30}$ glassy ribbons measured by VSM and B-H loop tracer. It is clear that the I_s decreases from 0.70 T to around 0.53 T with the addition of 2 at.% M element, as shown in inset (a). This glassy alloy system exhibits a high μ_e of (1.12–1.37) $\times 10^4$ at 1 kHz and a low H_c of 1.65–2.26 A m^{-1}, as shown in inset (b). Furthermore, good soft-magnetic properties in conjunction with a wide-range SCLR make these BMGs ideal candidates for the spark plasma sintering (SPS) process [17,18]. The SPS process can convert powders into the bulk form easily by the consolidation method, utilizing the significant viscous flow ability in the SCLR. The $(Co_{0.5}Fe_{0.5})_{62}Nb_6M_2B_{30}$ (M = Er, Tb, Y, Dy) BMG system exhibits an SCLR with a large range and good soft-magnetic properties, so that sintered specimens with a large size and a complex shape can easily be achieved.

Here we discuss the reasons why the $(Co_{0.5}Fe_{0.5})_{62}Nb_6M_2B_{30}$ (M = Er, Tb, Y, Dy) BMG system exhibits high thermal stability and good TPF ability. First, it is well known that Er, Tb, Y and Dy have large atomic radii, whereas a B atom has a small atomic radius of 0.09 nm [14]. The addition of M causes a significant change in the atomic sizes, resulting in an increase in the packing density of the supercooled liquid. Increasing the packing density of the supercooled liquid with low atomic diffusivity subsequently enlarges the SCLR. In addition, Er, Tb, Y and Dy have large negative heats of mixing with B and Co, and moderately negative heats of mixing with Fe [15]. The large mixing heats of the atomic pairs lead to an increase in the thermal stability of the supercooled liquid. Based on the DSC data, the addition of Er, Tb, Y and Dy can also effectively lead to a decrease in T_l, resulting in an increase in T_g/T_l. The increasing thermal stability of the supercooled liquid improves the GFA of the $(Co_{0.5}Fe_{0.5})_{62}Nb_6M_2B_{30}$ BMG system.

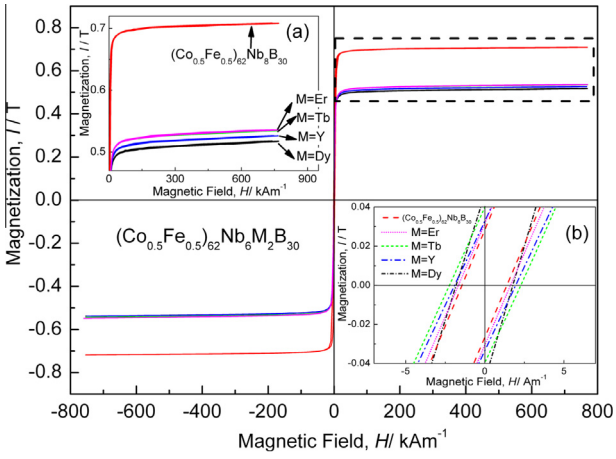

Figure 4. Hysteresis *I–H* curves of $(Co_{0.5}Fe_{0.5})_{62}Nb_6M_2B_{30}$ (M = Er, Tb, Y or Dy) and $(Co_{0.5}Fe_{0.5})_{62}Nb_8B_{30}$ glassy ribbons measured with VSM. (Inset a) Enlarged hysteresis curves of this alloy system; (inset b) hysteresis curves measured with a DC B–H loop tracer.

The high thermal stability of this BMG system offers a wide enough processing time window for the TPF process. On the other hand, the fragility parameter m, which refers to the steepness of the equilibrium temperature-dependent viscosity (η) at a temperature of T_g, is another key parameter for TPF [19]. For glass-forming liquids, the viscosity decreases dramatically with heating above the T_g. The molecular relaxation time increases with an Arrhenius-like form in strong liquids, and all others exhibit varying degrees of departure from Arrhenius behavior. In order to quantify the degree of departure from Arrhenius temperature dependence, the fragility parameter m was introduced [20]:

$$m = \left.\frac{d\log\langle\tau\rangle}{d\langle T_g/T\rangle}\right|_{T=T_g} \quad (1)$$

where $\langle\tau\rangle$ is the average relaxation time and T is the temperature. If $\langle\tau\rangle$ is given by the Vogel–Fulcher equation [21], then:

$$m = \frac{DT_0T_g}{(T_g - T_0)^2 \ln 10} \quad (2)$$

where D is the strength parameter in the Vogel–Fulcher equation, which controls how closely the liquid system obeys the Arrhenius law, and T_0 is the asymptotic value of T_g, usually approximated as the onset of the glass transition within the limit of an infinitely slow cooling and heating rate. The D and T_0 can be fitted by the Vogel–Fulcher equation [22]:

$$\ln\phi = \ln\ B - \frac{DT_0}{T_g - T_0} \quad (3)$$

where Φ is the heating rate and B is a parameter representing the timescale in the glass-forming system. It can be reasonably assumed that the larger m and ΔT_x for a given glass, the lower the viscosities that can be used for TPF. We measured the VFT relationship between T_g and the heating rate Φ of the $(Co_{0.5}Fe_{0.5})_{62}Nb_6Dy_2B_{30}$ BMG, and found fitting parameters ln B, D and T_0 of 8.07, 0.24 and 853 K, respectively. The value of the fragility parameter m evaluated at a heating rate of 20 K min^{-1} from Eq. (2) is 48. It is reported that most Zr-based BMGs are strong liquids with a value of m below 40; Pt- and Pd-based BMGs present intermediate values of m, with $41 \leqslant m \leqslant 66$ evaluated at a heating rate of 20 K min^{-1} [23]. The $(Co_{0.5}Fe_{0.5})_{62}Nb_6Dy_2B_{30}$ glass-forming liquid has intermediate fragility. It is thus concluded that the large SCRL and relatively high fragility parameter m lead to the high TPF ability of $(Co_{0.5}Fe_{0.5})_{62}Nb_6M_2B_{30}$ BMGs.

In summary, a BMG system of $(Co_{0.5}Fe_{0.5})_{62}Nb_6M_2B_{30}$ (M = Er, Tb, Y, Dy) glassy alloys with a large SCLR, a high σ_f, a strong TPF ability and good soft-magnetic properties was synthesized. The combination of good TPF ability and mechanical properties makes these ferromagnetic BMGs promising candidates for applications as structural and functional materials.

This work was supported by the National Natural Science Foundation of China (Grant No. 51271194), Ningbo Science and Technology Innovation Team (Grant No. 2011B82004), the National Basic Research Program of China (Grant No. 2010CB934602).

[1] G. Kumar, A. Desai, J. Schroers, Adv. Mater. 23 (2011) 461.
[2] A.L. Greer, Science 267 (1995) 1947.
[3] J.H. Na, W.T. Kim, D.H. Kim, S. Yi, Mater. Lett. 58 (2004) 778.
[4] K.F. Yao, C.Q. Zhang, Appl. Phys. Lett. 90 (2007) 061901.
[5] J. Schroers, T.M. Hodges, G. Kumar, H. Raman, A.J. Barnes, P. Quoc, T.A. Waniuk, Mater. Today 14 (2011) 14.
[6] G. Kumar, H.X. Tang, J. Schroers, Nature 457 (2009) 868.
[7] Y. Saotome, K. Itoh, T. Zhang, A. Inoue, Scr. Mater. 44 (2001) 1541.
[8] J. Schroers, Adv. Mater. 22 (2010) 1566.
[9] J. Schroers, T. Nguyen, S. O'Keeffe, A. Desai, Mater. Sci. Eng. A 449 (2007) 898.
[10] B. Zhang, D.Q. Zhao, M.X. Pan, W.H. Wang, A.L. Greer, Phys. Rev. Lett. 94 (2005) 205502.
[11] A. Inoue, B.L. Shen, H. Koshiba, H. Kato, A.R. Yavari, Nat. Mater. 2 (2003) 661.
[12] M.F. Ashby, A.L. Greer, Scr. Mater. 54 (2006) 321.
[13] A. Inoue, B.L. Shen, AIP Conf. Proc. 832 (2006) 11.
[14] Japan Inst. Metals (Ed.), Metals Databook, Maruzen, Tokyo, 1983, p. 8.
[15] F.R. de Boer, R. Boom, W.C.M. Mattens, A.R. Miedema, A.K. Niessen, Cohesion in Metals, Elsevier Science Publishers, Amsterdam, 1988, p. 224.
[16] Z.P. Lu, C.T. Liu, Acta Mater. 50 (2002) 3501.
[17] G.Q. Xie, D.V. Louzguine-Luzgin, H. Kimura, A. Inoue, Appl. Phys. Lett. 90 (2007) 241902.
[18] S. Lee, H. Kato, T. Kubota, A. Makino, A. Inoue, Intermetallics 17 (2009) 218.
[19] L.M. Martinez, C.A. Angell, Nature 410 (2001) 663.
[20] R. Böhmer, C.A. Angell, Phys. Rev. B. 45 (1992) 10091.
[21] R. Böhmer, K.L. Ngai, C.A. Angell, D.J. Plazek, J. Chem. Phys. 99 (1993) 4201.
[22] R. Brüning, K. Samwer, Phys. Rev. B 46 (1992) 11318.
[23] D.N. Perera, J. Phys. Condens. Matter. 11 (1999) 3807.